Effects of non-unity Lewis numbers in diffusion flames

By A. Liñán[1], P. Orlandi[2], R. Verzicco[2] AND F. J. Higuera[1]

The purpose of this work is to carry out direct numerical simulations of diffusion controlled combustion with non-unity Lewis numbers for the reactants and products, thus accounting for the differential diffusion effects of the temperature and concentration fields. We use a formulation (Liñán (1991a)) based on combining the conservation equations in a way to eliminate the reaction terms similar to the method used by Burke and Schumann (1928) for unity Lewis numbers. We present calculations for an axisymmetric fuel jet and for a planar, time evolving mixing layer, leaving out the effects of thermal expansion and variations of the transport coefficients due to the heat release. Our results show that the front of the flame shifts toward the fuel or oxygen sides owing to the effect of the differential diffusion and that the location of maximum temperature may not coincide with the flame. The dependence of the distribution of the reaction products on their Lewis number has been investigated.

1. Introduction

In many practical combustion systems reactions between fuel and oxidizer take place in thin reaction layers where the reactants meet at stoichiometric proportions, arriving by diffusion from opposite sides of the flame. In these systems the rate of burning is controlled by diffusion and not by the kinetics of the reaction, when the reaction is sufficiently fast. The turbulent character of the flow is an unavoidable requirement when we want to obtain large burning rates. The distorted and strongly corrugated form of the flames, when the flow is turbulent or even transitional, makes direct numerical simulation (DNS) of these flows very difficult.

The problem simplifies if we can assume that the Lewis numbers of the species, i.e. the ratios of their thermal to their mass diffusivities, are equal to unity. In this case we find combinations of species concentrations and temperature that are conserved in the reaction and are transported and diffuse like inert species. The assumptions of equal diffusivities and infinitely fast reaction have, therefore, been widely used for the description of diffusion controlled combustion after the pioneering work of Burke and Schumann (1928). See, for example, Delhaye *et al.* (1994) for a recent two-dimensional simulation of a spatially evolving mixing layer.

1 Escuela T. S. Ingenieros Aeronáuticos, Pza. Cardenal Cisneros 3, 28040 Madrid, Spain

2 Università di Roma, "La Sapienza", Dipartimento di Meccanica e Aeronautica, Via Eudossiana 18, 00184 Roma Italy

The purpose of the work described here has been to show how DNS of diffusion controlled combustion can be carried out for transitional flows with non-unity Lewis numbers using a generalization, given in Liñán (1991a) and Liñán and Williams (1993), of the Burke-Shumann procedure. Preliminary calculations have been made for an axisymmetric fuel jet in a stagnant oxidizer atmosphere and for a temporally evolving plane mixing layer, leaving aside in both cases the effect of thermal expansion. The results show some of the effects of the Lewis numbers on the flame location and on the temperature and product concentration.

Experimental work on reacting shear layers with nearly constant gas density has been performed by Mungal and Dimotakis (1984), Mungal, Hermanson and Dimotakis (1985), Masutani and Bowman (1986), and Mungal and Frieler (1988). Riley, Metcalfe and Orszag (1986) carried out three-dimensional simulations of a temporally evolving mixing layer with a single-step reaction whose rate does not depend on temperature, and much numerical work has been done subsequently on different aspects of reacting shear flows (see, for example, the Proceedings of previous Summer Programs). Models of scalar mixing and chemical reactions in turbulent mixing layers and jets have been proposed by Marble and Broadwell (1977), Broadwell and Breidenthal (1982), and Broadwell and Mungal (1991). See also the review by Bilger (1989)

2. Formulation

We assume that an infinitely fast reaction, with the overall stoichiometry

$$F + rO_2 \rightarrow (1+r)P + (q) \tag{1}$$

is taking place in the thin reaction zone so that a mass of oxygen, r, is consumed and a mass of products, $(1+r)$, is generated together with a thermal energy per unit mass of fuel consumption, q.

If D_T, D_T/L_F, D_T/L_O, and D_T/L_P are the thermal and mass diffusivities of the fuel, oxygen, and products (written in terms of the corresponding Lewis numbers), we can form combinations of the conservation equations for the species and the energy where the reaction terms are eliminated. Thus, if Y_F and Y_O are the mass fractions of the fuel and of the oxygen, we can derive the conservation equation

$$\rho\frac{D}{Dt}(rY_F - Y_O) - \nabla\cdot\rho D_T\nabla(rY_F/L_F - Y_O/L_O) = 0, \tag{2}$$

where the reaction term is absent. This equation can be written in the form

$$L_m\rho\frac{D}{Dt}Z - \nabla\cdot(\rho D_T\nabla\widetilde{Z}) = 0, \tag{3}$$

which uses the traditional mixture fraction

$$Z = (S\widehat{Y}_F - \widehat{Y}_O + 1)/(1+S), \tag{4a}$$

based on the Schvab-Zeldovich coupling function appearing in the material derivative term of Eq. (2) and the modified mixture fraction $\tilde{Z}$, defined by

$$\tilde{Z} = (\tilde{S}\hat{Y}_F - \hat{Y}_O + 1)/(1 + \tilde{S}), \tag{4b}$$

based on the coupling function appearing in the diffusion term of Eq. (2), where the mean Lewis number is defined as $L_m = L_O(1 + S)/(1 + \tilde{S})$. In these relations $\hat{Y}_F = Y_F/Y_{F0}$, $\hat{Y}_O = Y_O/Y_{O0}$ are the mass fractions scaled by their free-stream values, and $S = rY_{F0}/Y_{O0}$ and $\tilde{S} = SL_O/L_F$ are air/fuel mass stoichiometric ratios. Notice that the combination $(rY_F/L_F - Y_O/L_O)$ and its gradient, and therefore $\tilde{Z}$ and grad $\tilde{Z}$, are continuous in the thin flame, where we have a reaction-diffusion balance. The gradient of Z, on the other hand, has a jump in the reaction sheet.

In a similar fashion to the conservation equation for the mixture fraction, we can write a conservation equation

$$\rho L_P \frac{DY}{Dt} - \nabla \cdot (\rho D_T \nabla Y) = (L_P - L_F)\rho \frac{DY_F}{Dt} + (L_P - L_O)\rho \frac{DY_O}{Dt} \tag{5}$$

for the 'potential' product mass fraction

$$Y = \hat{Y}_F + \hat{Y}_O + \frac{1 + \tilde{S}}{1 + r} \frac{L_F}{L_P} \frac{Y_P}{Y_{F0}}, \tag{6}$$

and the conservation equation

$$\rho \frac{DH}{Dt} - \nabla \cdot (\rho D_T \nabla H) = (1 - L_F)\rho \frac{D\hat{Y}_F}{Dt} + (1 - L_O)\rho \frac{D\hat{Y}_O}{Dt} \tag{7}$$

for the reduced total enthalpy

$$H = \hat{Y}_F + \hat{Y}_O + c_p(T - T_0)L_F \frac{1 + \tilde{S}}{qY_{F0}}. \tag{8}$$

Here we have assumed a constant specific heat c_p and used the low Mach number approximation for the energy equation. Eqs. (3), (5)m and (7) must be complemented by the equations of state, continuity and momentum conservation, in addition to the Burke-Schumann equilibrium condition: $\hat{Y}_F = 0$ on the air side of the flame and $\hat{Y}_O = 0$ on the fuel side. Namely, by the relations

$$\hat{Y}_F = 0, \quad 1 - \hat{Y}_O = Z/Z_S = \tilde{Z}/\tilde{Z}_S \tag{9a}$$

where $Z < Z_S = 1/(1 + S)$ or $\tilde{Z} < \tilde{Z}_S = 1/(1 + \tilde{S})$, and

$$\hat{Y}_O = 0, \quad \hat{Y}_F = (Z - Z_S)/(1 - Z_S) = (\tilde{Z} - \tilde{Z}_S)/(1 - \tilde{Z}_S) \tag{9b}$$

where $\widetilde{Z} > \widetilde{Z}_S$. The flame lies on the stoichiometric mixture fraction level surface where $\widetilde{Z} = \widetilde{Z}_S$. Thus $\widetilde{Z}$ is given by Eq. (3) complemented by the piecewise linear relation $Z(\widetilde{Z})$ given by Eqs. (9). If $L_F = L_O$ then $Z \equiv \widetilde{Z}$.

The temperature and product concentrations are given, using Eqs. (9), by H and $\widetilde{Z}$, and Y and $\widetilde{Z}$, according to Eqs. (6) and (8). H and Y are given by eqs. (5) and (7), where the differential diffusion effects, represented by the terms in the right hand side of the equations, can be written in terms of $\widetilde{Z}$.

The boundary conditions to be used include $Z = H - 1 = Y - 1 = 0$ on the air feed stream and $Z - 1 = H - H_F = Y - 1 = 0$ on the fuel feed stream, with $H_F = 1 + c_p(T_F - T_O)(1 + \widetilde{S})/qY_{F0}$ in terms of the fuel and air feed stream temperatures T_F and T_O.

We have carried out calculations of the flow field without taking into account the effects of variable density or variable transport coefficients associated with the exothermicity of the reaction. The emphasis here has been placed on non-unity Lewis number effects, while the companion paper by Higuera and Moser (this issue) deals with the effects of thermal expansion and variable diffusivity for the equi-diffusional case.

The mixture fraction field, as well as the concentration fields of the fuel and oxygen, given in terms of $\widetilde{Z}$ by relations (9*a*) and (9*b*), are dependent on the parameters L_F, L_O and $\widetilde{S} = SL_F/L_O$. In all of our calculations we have used the reasonable assumption $L_O = 1$ and have considered $T_F = T_O$ and some representative values of L_F and of the mass stoichiometric ratio $S = rY_{F0}/Y_{O0}$.

Eqs. (5) and (7), giving the reduced total enthalpy H and the potential product concentration Y, are identical if the Lewis number L_P of the product is 1. If the initial temperature of the fuel is equal to that of the ambient air, then, the boundary conditions are also identical and the values of $c_p(T - T_0)/q$ and $Y_P/(1+r)$ are equal.

We have determined the product concentration for values of $L_P \neq 1$. The product concentration has been scaled with the constant value, $Y_{F0}(1 + r)/(1 + S)$, of the product mass fraction along the flame sheet when all the Lewis numbers are equal to the unity; in this equi-diffusional case, the flame temperature is constant and equal to the adiabatic flame temperature $T_e = T_0 + qY_{F0}/[c_p(1 + S)]$.

Due to the so called differential diffusion effects (effects of non-unity Lewis numbers) we may expect the flame temperature to vary in the range between T_e and $T_d = T_0 + qY_{F0}/[c_pL_F(1 + \widetilde{S})]$; the last value corresponding to cases where diffusion is dominant over convection and local accumulation. Similarly, the product mass fraction along the flame sheet should vary between $Y_{F0}(1 + r)/(1 + S)$ and $Y_{F0}(1 + r)(L_P/L_F)/(1 + \widetilde{S})$. Notice, however, that the total product generation in the flame will not be dependent on the diffusivity of the product, but on $\widetilde{S}$ and L_F, because in these constant density calculations the product generation is controlled by the diffusion of the reactants to the flame sheet.

3. Simulations of jet diffusion flames

Before performing the simulation of a space developing axisymmetric jet, the

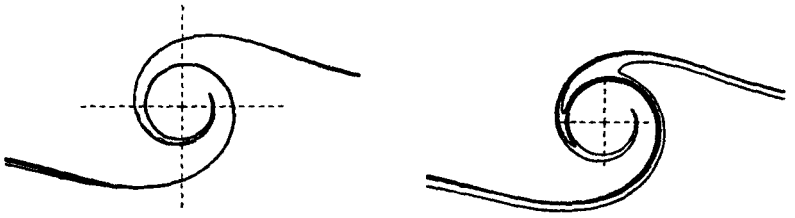

a) *b)*

FIGURE 1. Contour plots of the stoichiometric mixture fraction $Z_S = 0.272$ ($L_O = 0.8$, $L_F = 1.2$, and $r = 5$) for the Marble problem: *a)* $Pe = 5000$ lines are superimposed for $t = 4$, $t = 8$, $t = 12$, $t = 16$, and $t = 20$, *b)* solutions at $t = 20$ for $Pe = 100$, $Pe = 500$, $Pe = 1000$, and $Pe = 5000$. $Pr = 0.72$ in all cases. The crossing of —·— lines indicates the center of the vortex.

numerics related to the solution of Eqs. (3) and (5) have been checked by investigating whether the numerical solution reproduces the self-similar behavior of the mixture fraction Z when it is advected and diffused by a point vortex of circulation Γ (Marble problem). This problem has been theoretically studied by Liñán (1991b) for non-unity Lewis numbers. Since in the numerical simulation we could not use a point vortex, we considered a Rankine vortex (i.e. a vortex with $\omega = const$ for $r \leq \sigma$ and $\omega = 0$ for $r > \sigma$) of core size $\sigma = 0.1$ and unity circulation. It is clear that with this approximation the self-similar solution does not hold for $t = 0^+$ but only after a certain transient. This simulation was necessary to investigate whether our finite difference scheme could handle different variables in the right-hand and the left-hand sides of Eq. (3) ($\widetilde{Z}$ and Z respectively) since due to stability reasons an implicit discretization of the right-hand side of Eq. (3) has been used. Numerical difficulties could arise from the fact that in the reaction sheet there is a jump in the grad Z. In our numerical resolution a variable χ was introduced ($Z = \widetilde{Z}/\chi$) with χ given by the comparison of Eq. (4*a*) and (4*b*) with the Burke-Schumann condition in the oxygen and fuel regions. By this transformation in the left-hand side, the time derivative $\partial Z/\partial t$ is substituted by $\partial(\widetilde{Z}/\chi)\partial t$ and the equation is thus discretized as for the momentum equations.

In Fig. 1a the distributions of the line $Z_S = 0.25$ are given for a value of $Pe \equiv \Gamma/D_T = 5000$ at different times in terms of the coordinates $x = \eta\cos(\theta)$ and $y = \eta\sin(\theta)$ with $\eta = r/\sqrt{(\Gamma t/2\pi)}$ the similarity variable, r and θ being radial and azimuthal coordinates in the physical domain. The oscillations inside the spiral of Fig. 1*a*, observed at $t = 4$, are due to the grid (129 × 129) which is not fine enough to represent the very sharp gradients at this Pe. These oscillations disappear due to diffusivity, and the solution reaches a self-similar distribution where advection is balanced by diffusivity. In Fig. 1b the self-similar solutions at different Pe are shown and these solutions compare well with the theoretical results obtained by Liñán.

Having verified that the numerical method can satisfactorily deal with non-unity Lewis numbers, we move on to more realistic computations of a fuel jet exhausting into stagnant air. In what follows we use the mean exhaust velocity and the radius a of the exhaust pipe as units of velocity and length. The Reynolds number based on these quantities is $Re = 2500$ for the simulations presented in this section, this value being a limit fixed by the present computer's limitations. The injection velocity is uniform except for a thin boundary layer with a momentum thickness of roughly $a/60$. This inlet velocity profile is very similar to the one of the Longmire & Eaton experiment, which produced a vortex shedding with a Strouhall number $St = 0.5$. Several simulations were performed without combustion in order to find under what conditions the jet can sustain the continuous formation of vortex rings without any inlet perturbation. It was observed that the outer boundary should be located at a certain minimum distance from the symmetry axis to have a Strouhall number in agreement with that in the experiments of Longmire & Eaton (1992).

Fig. 2 shows the results of three simulations of a methane jet in air for which $r = 4$, $Y_{O0} = 0.23$, and $L_F = 0.8$ at a time $t = 70$ after the onset of injection. The figure includes the vorticity field, common to all the simulations, and the position of the flame for $\widetilde{Z}_S = 0.46$, 0.166, and 0.044, corresponding to $\widetilde{S} = 0.92$, 4, and 17.4, which in turn are obtained by setting Y_{F0} equal to 0.053, 0.23, and 1. Notice how with increasing value of the stoichiometric ratio $\widetilde{S}$ the flame moves toward the air side, out of the region of strong shear.

In these simulations there are source terms in the right hand sides of Eqs. (5)-(7) which arise due to the effect of the differential diffusion. These terms can not be checked by theoretical considerations as done before for the Z equation; however, an obvious physical requirement is that no negative values of $\widehat{Y}_F$ and of $\widehat{Y}_O$ should occur. Negative concentrations did indeed appear in our preliminary computations during the early stages of the flow (not displayed) when the front of the jet is moving into the air and the gradients are very steep. However, these unphysical transient oscillations disappear when the round jet is formed.

In Fig. 3 the variation of the fuel flux, scaled with its inlet value, is given for the three cases mentioned before, showing as expected that in the case of very diluted fuel the flux decreases faster than in the other cases. This figure shows that the fuel is mainly accumulated within the vortices and depleted in the braid regions. We observe furthermore the large accumulation of fuel in the last vortex formed by pairing of previous vortices. This means that as a result of the combustion the cores of the vortices run out of oxygen, and large quantities of unburned fuel are transported far from the injection place due to the convection of the vortices themselves. We did not observe complete fuel consumption in these simulations because of the limited extension of the domain in the downstream direction. Simulations will be carried out in the future with a longer domain to investigate this issue. Plots of the corresponding scaled product concentration for $L_p = 1$ are shown in Fig. 4, showing that the location of the maximum generation of products coincides with the location of maximum fuel consumption. We have also evaluated but not plotted here the mixture fraction gradient, and we observe that it has the largest values

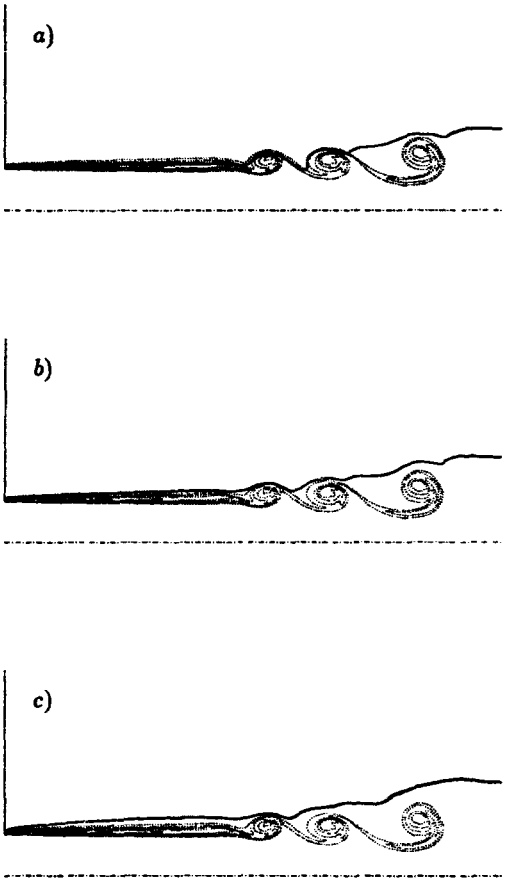

FIGURE 2. Countour plots of the azimuthal vorticity (·····)for the jet at $t = 70$ and $Re = 2500$, $Pr = 0.72$. Contour increment $\Delta = 0.5$. Thick solid line is the flame position: *a*) $\widetilde{Z}_S = 0.46$, *b*) $\widetilde{Z}_S = 0.166$, *c*) $\widetilde{Z}_S = 0.044$.

in the braid regions where we find also the largest values of the concentration of the products. The gradient of Z evaluated at the flame sheet measures the burning rate per unit flame flame surface. If it exceeds a critical value, the flame would be locally extinguished according to the analysis of Liñán (1974). (See Givi, Jou and Metcalfe (1986) for numerical work on flame extinction in a temporally evolving

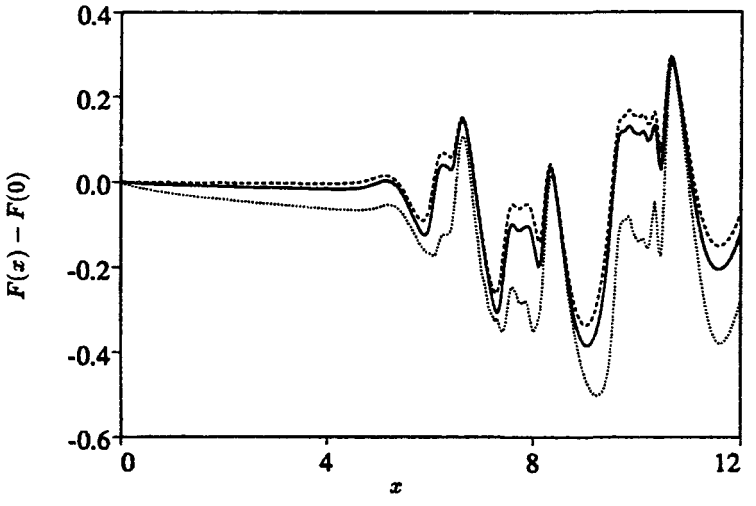

FIGURE 3. Axial profile of the fuel flux (reduced by its value at the inlet) for the simulations shown in Fig. 2: ---- $S = 17.4$, —— $S = 4$, ····· $S = 0.92$.

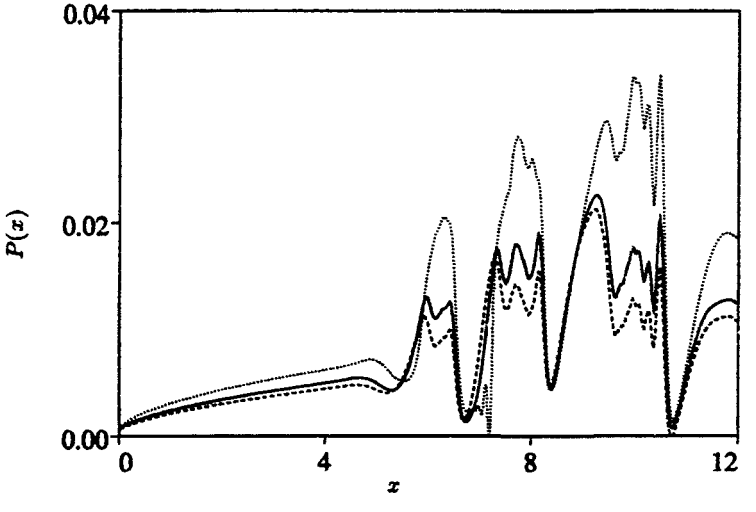

FIGURE 4. Axial profile of the products flux for the simulations shown in Fig. 2: ---- $S = 17.4$, —— $S = 4$, ····· $S = 0.92$.

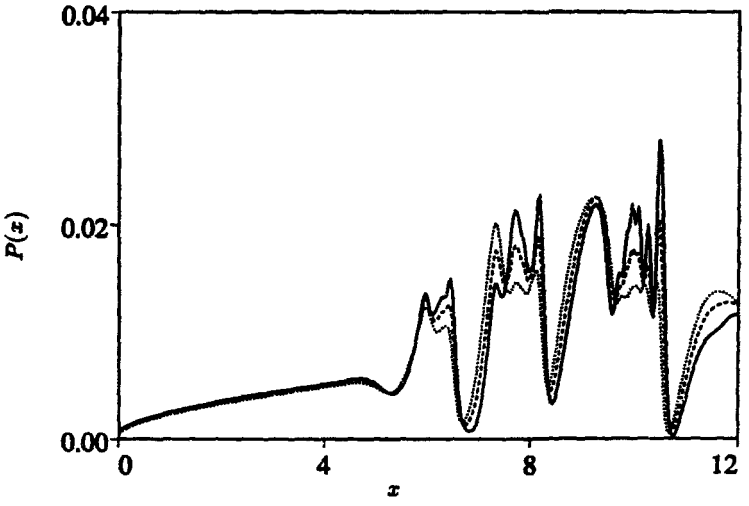

FIGURE 5. Axial profile of the products flux for $\widetilde{S} = 4$. —— $L_P = 0.8$, ---- $L_P = 1$, ····· $L_P = 1.2$.

mixing layer.)

To investigate the effect of the products Lewis number on the distribution of the concentration of the products we have performed simulations with $L_P = 0.8$ and with $L_P = 1.2$. As indicated before, the contour levels of the product concentration for $L_P = 1$ also give the temperature levels. Fig. 5 shows for the case $Y_{F0} = 0.23 = Y_{O0}$ that the products, which are mainly generated in the braid regions at a rate independent of their diffusivity, are more concentrated in the eddies when L_P is larger, thus leading to stronger variations of the product flux when the eddies travel past a given station.

4. Temporally evolving mixing layer

Two-dimensional simulations of a temporally evolving mixing layer have been carried out using as initial conditions the base profiles

$$u = \mathrm{erf}(\sqrt{\pi}y) \quad \text{and} \quad \begin{cases} \dfrac{\widetilde{Z}}{\widetilde{Z}_S} = \dfrac{\mathrm{erfc}(\sqrt{\pi Pr L_O}\, y)}{\mathrm{erfc}(\sqrt{\pi Pr L_O}\, y_f)} & \text{for } \widetilde{Z} < \widetilde{Z}_S \\ \dfrac{1-\widetilde{Z}}{1-\widetilde{Z}_S} = \dfrac{1+\mathrm{erf}(\sqrt{\pi Pr L_F}\, y)}{1+\mathrm{erf}(\sqrt{\pi Pr L_F}\, y_f)} & \text{for } \widetilde{Z} > \widetilde{Z}_S \end{cases} \qquad (10a-b)$$

plus initial perturbations proportional to the eigenfunctions of the most unstable small perturbation of the error function velocity profile and its subharmonic. Here y_f, the position of the flame, verifies

$$1 + \mathrm{erf}(\sqrt{\pi Pr L_F}\, y_f) = \left(\frac{L_F}{L_O}\right)^{1/2} \frac{1-\widetilde{Z}_S}{\widetilde{Z}_S} \mathrm{erfc}(\sqrt{\pi Pr L_O}\, y_f) e^{-\pi Pr (L_F - L_O) y_f^2}$$

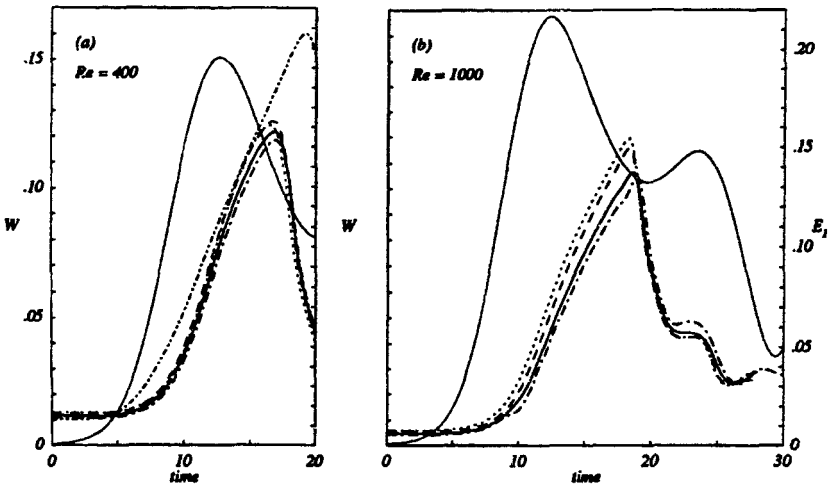

FIGURE 6. Overall rate of product generation for: (a) $Re = 400$. ——— : $L_F = 1$, $S = 9$ ($\widetilde{S} = 9$). - - - - : $L_F = 0.8$, $S = 7.2$ ($\widetilde{S} = 9$). ····· : $L_F = 0.8$, $S = 9$ ($\widetilde{S} = 11.25$). —·— : $L_F = 1.2$, $S = 10.8$ ($\widetilde{S} = 9$). —··— : $L_F = 1$, $S = 1$ ($\widetilde{S} = 1$). (b) $Re = 1000$. ——— : $L_F = 1$, $S = 9$ ($\widetilde{S} = 9$). - - - - : $L_F = 0.5$, $S = 4.5$ ($\widetilde{S} = 9$). —·— : $L_F = 1.5$, $S = 13.5$ ($\widetilde{S} = 9$). ····· : $L_F = 0.5$, $S = 4.5$ ($\widetilde{S} = 9$) with the initial conditions of $L_F = 1$. The thin curves to be read off the scales to the right represent the first mode of the kinetic energy spectrum.

which, for $\widetilde{Z}_S \gg 1$, yields

$$y_f \approx \frac{1}{\sqrt{\pi Pr L_F}} \left\{ \ln \left[\frac{S}{2\sqrt{\pi}} \frac{1}{\sqrt{\ln \frac{S}{2\sqrt{\pi}}}} \right] \right\}^{1/2}$$

Eqs. (10) and similar expressions for the total enthalpy and the potential product mass fraction correspond to the parallel flow resulting from the evolution of a half-space ($y < 0$) filled with $\widehat{Y}_O = 0$, $\widehat{Y}_F = 1$ and a half-space ($y > 0$) filled with $\widehat{Y}_O = 1$, $\widehat{Y}_F = 0$, moving initially with opposite velocities. Hereafter velocities are scaled with half this velocity difference, and distances with the vorticity thickness of the basic flow (10a). $Pr = 1$ in the simulations.

Fig. 6a shows the overall rate of product generation,

$$W = \frac{1}{L} \frac{d}{dt} \int \widehat{Y}_F \, dx \, dy$$

where $\widehat{Y}_P$ is the scaled product concentration and L is the streamwise length of the computational domain for a number of simulations with $Re = 400$ and a time interval covering a vortex roll-up. To establish a common basis for comparison, the same initial $\widetilde{Z}$ was used in all the simulations, corresponding to the base profile (10b) with $Pr = L_F = L_O = 1$. As can be seen, the rate of product generation peaks after roll-up in all the cases computed, the peak value being the highest in the only case displayed with $\widetilde{S} = 1$ (and similar to those of other cases not displayed with $L_F \neq 1$ and $\widetilde{S}$ about 1). This is because the flame sheet then lies inside the region of high vorticity and, in the absence of density changes that might alter the flow, large portions of the flame are subject to high strain rates that increase its surface and the fluxes of the reactants toward it. The other curves in Fig. 6a correspond to higher values of $\widetilde{S}$, for which the peak values increase with decreasing L_F or decreasing S. In the following we give some tentative explanations of these results.

The weak dependence of the rate of product generation on the Lewis number of the fuel when $\widetilde{S}$ is kept constant can be understood by noticing that, in the absence of molecular transport, each material particle would conserve its initial temperature and mass fractions of fuel and oxygen so that the fields of these variables as well as the position and shape of the flame would not change. In particular, the values of $\nabla\widehat{Y}_O$ and $\nabla\widehat{Y}_F$ at the flame would not depend on L_F, but the diffusion flux of fuel, $-L_F^{-1}\nabla\widehat{Y}_F$, would. What happens is that the stoichiometric ratio S is changing with L_F to keep $\widetilde{S}$ constant; S decreases when L_F decreases, and the flame then requires more fuel to consume the same amount of oxygen, generating more products. The variation, however, is small if S is large because the product generation is then essentially determined by the consumption of oxygen.

Similarly, to understand the weak dependence of the rate of product generation on the stoichiometric ratio, notice that for large values of S, the flame sits in a region where the modified mixture fraction is decaying exponentially, and according to (10b), a $|\nabla\widetilde{Z}|_{flame} = O(y_f\widetilde{Z}_S)$, with $y_f = O(\ln \widetilde{Z}_S^{-1})$ and $\widetilde{Z}_S = 1/(1+\widetilde{S})$, should be expected. Hence a decrease of S at constant L_F is accomodated with only a small shift of the flame, whereas $\nabla\widehat{Y}_O = -(1+\widetilde{S})\nabla\widetilde{Z}$ remains practically constant and $\nabla\widehat{Y}_F \approx \nabla\widetilde{Z}$ increases. As before, this implies a weak increase of the rate of product generation.

Further computations were carried out with $Re = 1000$ and a time interval covering the first pairing to assess the influence of the molecular transport on the previous results and to study the evolution after the roll-up of the vortices. Rather extreme values of L_F were chosen to exaggerate the effect of this parameter, and initial conditions (10b) with both $L_F = 1$ and L_F equal to the values actually used in the computations were considered in an attempt to describe the influence of this factor. The results, in Fig. 6b, have the same appearance as cases with the smaller Reynolds number, with slightly lower peak values of the rate of product generation. No further peaks appear during the pairing process.

Fig. 7 shows the temperatures for $L_F = 0.5$ and 1.5 as well as the vorticity and the flame positions during the first pairing of the vortices. The maximum temperature

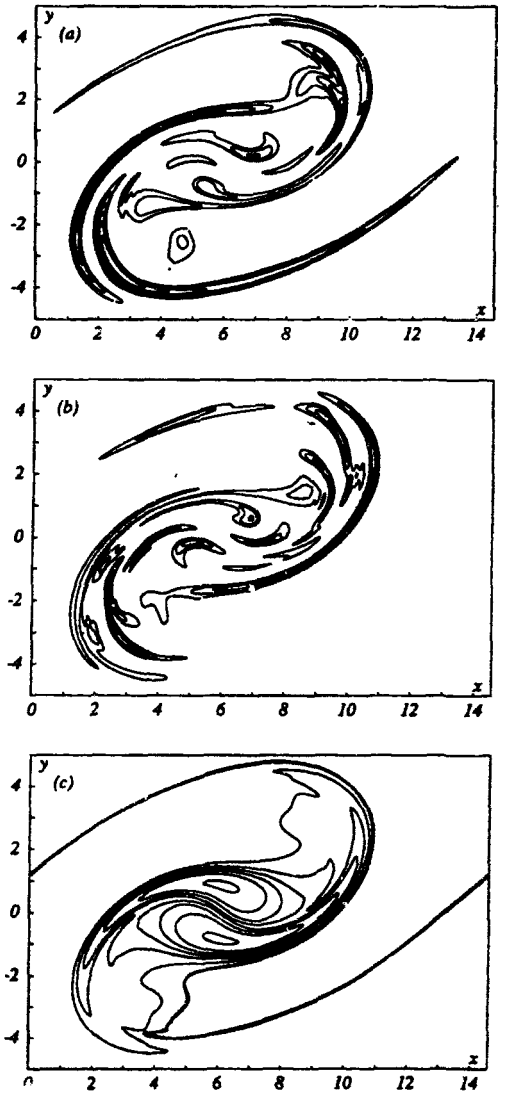

FIGURE 7. Results for $Re = 4000$ at $t = 38$. (*a*.) Temperature field for $L_F = 0.5$. (*b*.) Temperature field for $L_F = 1.5$. (*c*.) Vorticity field and position of the practically coinciding flames for $L_F = 0.5$ and 1.5.

in these pictures is attained at points separated from the flame, a consequence of the differential diffusion acting in thin layers that were around the flame at earlier times.

5. Conclusions

The work carried out has shown the feasibility of direct numerical simulations of diffusion controlled combustion with non-unity Lewis numbers of reactants and products. In the calculations we have left out the effects of thermal expansion and variations of the transport coefficients due to heat release. The preliminary calculations should be extended in the future to include effects of heat release, and a more systematic analysis should be carried out to verify or extend the tentative conclusions presented here.

REFERENCES

BILGER, R. W. 1989 Turbulent diffusion flames. *Ann. Rev. Fluid Mech.* **21**, 101–135.

BROADWELL, J. E. & BREIDENTHAL, R. E. 1982 A simple model of mixing and chemical reaction in a turbulent shear layer. *J. Fluid Mech.* **125**, 397–410.

BROADWELL, J. E. & MUNGAL, M. G. 1991 Large-scale structures and molecular mixing. *Phys. Fluids A.* **3**, 1193–1206.

BURKE, S. P. & SCHUMANN, T. E. W. 1928 Diffusion flames. *Industr. Eng. Chem.* **20**, 998–1004.

DELHAYE, Б., VEYNANTE, D. & CANDEL, S. M. 1994 Simulation and modeling of reactive shear layers. *Theoret. Comput. Fluid Dynamics.* **6**, 67–87.

GIVI, P., JOU, W.-H. & METCALFE, R. W. 1986 Flame extinction in a temporally developing mixing layer. Proc. 21nd. Int. Symp. Combustion, 1251–1261. The Combustion Institute, Pittsburgh.

KATTA, V. R., GOSS, L. P. & ROQUEMORE, W. H. 1994 Effect of non-unity Lewis number and finite rate chemistry of a H_2/air jet diffusion flame. *Comb. & Flame.* **96**, 60–74.

LIÑÁN, A. 1974 The asymptotic structure of laminar diffusion flames for large activation energies. *Astronautica Acta.* **1**, 1007-1031.

LIÑÁN, A. 1991a The structure of diffusion flames. In Fluid Dynamical Aspects of Combustion theory. Ed. by Onofri, M. & Tesev, A. Longman Scientific & Technical, 11-29.

LIÑÁN, A. 1991b El papel de la Mecánica de Fluidos en los Procesos de Combustión. (In Spanish). Real Academia de Ciencias, Madrid, Spain.

LIÑÁN, A. & WILLIAMS, F. A. 1993 Fundamental Aspects of Combustion. Oxford Univ. Press.

LONGMIRE, E. K. & EATON, J. K. 1992 Structure of a particle-laden round jet. *J. Fluid Mech.* **236**, 217–257.

MAHALINGAM, S., CANTWELL, B. J. & FERZIGER J. H. 1990 Full numerical simulation of co-flowing axisymmetric jet diffusion flames. *Phys. Fluids A.* **2**, 720-728.

MARBLE, F. & BROADWELL, J. E. 1977 The coherent flame model for turbulent chemical reaction. Report No. TRW-9-PU. Project SQUID.

MASUTANI, S. M. & BOWMAN, C. T. 1986 The structure of a chemically reacting plane mixing layer. *J. Fluid Mech.* **172**, 93–126.

MUNGAL, M. G. & DIMOTAKIS, P. E. 1984 Mixing and combustion with low heat release in a turbulent shear flow. *J. Fluid Mech.* **148**, 349–382.

MUNGAL, M. G. & FRIELER, C. E. 1988 The effects of Damköhler number in a turbulent shear layer. *Comb. Flame.* **71**, 23–34.

MUNGAL, M. G., HERMANSON, J. C. & DIMOTAKIS, P. E. 1985 Reynolds number effects on mixing and combustion in a reacting shear layer. *AIAA J.* **23**, 1418–1423.

RILEY, J. J., METCALFE, R. W. & ORSZAG, S. A. 1986 Direct numerical simulations of chemically reacting turbulent mixing layers. *Phys. Fluids.* **29**, 406–422.